Direct observation of electron propagation and dielectric screening on the atomic length scale

S. Neppl[1,2], R. Ernstorfer[3], A.L. Cavalieri[4], C. Lemell[5], G. Wachter[5], E. Magerl[2], E.M. Bothschafter[6], M. Jobst[1,2], M. Hofstetter[2,6], U. Kleineberg[2,6], J.V. Barth[1], D. Menzel[1,3], J. Burgdörfer[5], P. Feulner[1], F. Krausz[2,6] and R. Kienberger[1,2]

1 Physikdepartment, Technische Universität München, 85747 Garching, Germany

2 Max-Planck-Institut für Quantenoptik, Hans-Kopfermann-Str. 1, *85748 Garching, Germany*

3 Fritz-Haber-Intstitut der Max-Planck-Gesellschaft, 14195 Berlin, Germany

4 Max Planck Institute for the Structure and Dynamics of Matter, Luruper Chaussee 149, 22761 Hamburg, Germany

5 Institute for Theoretical Physics, Vienna University of Technology, A-1040, Vienna, Austria, EU

6 Fakultät für Physik, Ludwig-Maximilians-Universität München, Am Coulombwall 1, D-85748 Garching, Germany

The propagation and transport of electrons in crystals is the most fundamental process pertaining to the functioning of most electronic devices. Microscopic theories describe this phenomenon based on the motion of Bloch wave packets[1]. They are localized in the reciprocal space with a group velocity given by the dispersion of the electronic band structure near the central wavevector k_0 of the wave packet. This concept has been verified experimentally in superlattices by the observation of Bloch oscillations[2], i.e. periodic oscillations of electrons in real and reciprocal space. Here, we present a direct observation of electron wave packet motion in a real-space and real-time experiment, on length and time scales shorter than the Bloch oscillation amplitude and period. We show that attosecond metrology[3] now enables quantitative insight into weakly disturbed electron wave packet propagation on the atomic length scale without being hampered by scattering effects, which inevitably occur over macroscopic propagation length scales. We use sub-femtosecond extreme ultraviolet (XUV) light pulses[2,4] to launch photoelectron wave-packets inside a tungsten crystal which is covered by few-angstrom-thick magnesium films of variable thickness[5]. Probing their moment of arrival at the surface with attosecond (1 as = 10^{-18} s) precision reveals free-electron-like, ballistic propagation behavior inside the adlayer material - the semi-classical limit of Bloch wave-packet motion. Real-time access to electron transport through atomic layers and interfaces affords promise of unprecedented insight into phenomena of pivotal importance for scaling electronic and photonic circuits towards atomic dimensions. In addition, our experiment sheds light on the atomic-scale screening of optical fields at solid interfaces and allows for determining the penetration depth of electrical fields on this exact length-scale.

A detailed microscopic understanding and control of electronic and optical properties of solids depends on our ability to access the dynamics of electrons on atomic time and length scales. Tracking the propagation of electrons in real time requires the ability to pinpoint their position at a rate comparable to the time on which interactions with other electrons and the crystal lattice may affect their trajectories inside the material. In a classical picture, the upper bound for the necessary temporal resolution is therefore the time it takes the electrons to travel the several-Angstrom distance between neighbouring atoms. This implies transit times well below 1 femtosecond even for kinetic energies as low as E_{kin} ~1 eV. Previous time-resolving studies on electron propagation in condensed matter employed laser-based spectroscopic techniques to reveal ballistic currents and drift motion of charge carriers[6-9]. Restricted to the pico- and femtosecond time scale, they are capable to probe carrier dynamics averaged over several hundreds of nanometers. In contrast, the experimental approach demonstrated here offers quantitative real-time access to electron transport on the inter-atomic length scale.

Figure 1 illustrates the basic principle of the experiment. Attosecond XUV light pulses generate Bloch electron wave-packets with energies significantly above the vacuum level. Electron wave packets with a sufficiently large momentum component along the surface-normal direction z contribute to the photoelectron current reaching the time-of-flight detector (TOF). Conventional photoelectron spectroscopy is restricted to measure energy and momentum distributions of photoelectrons. We additionally capture the temporal profile of the photoemission process by having the ejected electrons interact with the controlled few-cycle electric field of a visible/near-infrared (VIS/NIR; 500 – 1000 nm; in the following simply referred to as NIR) laser pulse phase-locked to the ionizing XUV pulse. As this field modifies (“streaks”) the momentum of a photoelectron in proportion to the laser vector

potential $A_L(z,t)$ at the instant t the electron enters the NIR field[3,11], the temporal profile of the electron wave packet leaving the sample is mapped onto its final momentum distribution. Full streaking spectrograms obtained by recording these laser-modulated electron-energy distributions as a function of delay Δt between the XUV and the NIR pulse are therefore highly sensitive to the spatio-temporal characteristics of both the photoelectron wave packet and the streaking laser field on angstrom length and the attosecond time scale[12].

Direct (time-domain) access to these electronic and optical wave packets promises a unique insight into the photoelectric effect[13], including underlying electron propagation and phenomena as fundamental as dielectric screening of light fields at solid surfaces. Here we show that this can be achieved by combining state-of-the-art attosecond timing metrology (chronoscopy)[3,10-12] with sample engineering on the angstrom level[5,13].

When excited from Bloch states inside the crystal to positive-energy states[14], photoelectrons are not immediately exposed to the streaking field as the latter is screened at the surface. Therefore, the time delay associated with the propagation of the respective Bloch wave packets towards the surface (included in both the quantum-mechanical one-step[14] and the semi-classical three-step[15,16] description of photoemission) is encoded in the streaking spectrogram[12]. Differences in the propagation time of electrons ejected from different initial Bloch states manifest themselves as a temporal offset between the respective streaking traces[10-12] (cf. Fig. 1a). Previous studies on single crystals revealed a considerable time delay between the emission of core-level and conduction band (CB) photoelectrons from the transition metal W(110)[10], whereas such a delay was found to be absent in the photoemission from the free-electron metal Mg(0001)[11]. Theoretical models have addressed different contributions such as the band structure of the material[10,17,18], the spatial characteristics of

the initial-state wave functions[19-22], elastic and inelastic scattering effects[10,23], and the screening behavior of the laser field at the surface[20,23,24] to the photoemission time delays measured by attosecond streaking. In order to isolate the atomic-scale electron propagation process from this multitude of disparate effects, we investigate hybrid metallic samples consisting of a controllable number, n, of magnesium (Mg) adlayers on a tungsten W(110) crystal[13,25] (see Fig. 1a and supplementary information, SI, for details) and contrast the measured time shifts with electron transport calculations.

In our experiments, XUV pulses with a duration of about 450 as carried at a photon energy of $\hbar\omega_{XUV}$ = 118 eV simultaneously generate photoelectrons from core states of the substrate (W4*f*) and adlayer (Mg 2*p*), as well as from the energetically overlapping CB states of both materials (Fig. 1b). A representative streaking spectrogram for n = 4 Mg adlayers on W(110) is shown in Fig. 2a. Despite the significant attenuation of the tungsten substrate photoemission due to inelastic scattering in the Mg overlayer, the streaked W4*f* and CB photoemission lines are well discernible. They are also sufficiently separated from each other and from the Mg2*p* line over the entire range of XUV-NIR delays, Δt, which guarantees an accurate quantitative analysis of their relative emission dynamics[10-12]. In what follows, we reference the emission times of the W4*f* and CB electrons to the Mg2*p* emission from the Mg overlayer and denote the resultant relative delays as $\Delta\tau$[4*f* - 2*p*] and $\Delta\tau$[CB - 2*p*], respectively.

We begin with an analysis of $\Delta\tau$[4*f* - 2*p*] because the involved photoelectrons originate from atomic-like states that are entirely localized in the W(110) substrate or the Mg overlayer. This allows unambiguous interrelation of the measured time shifts and the well-defined propagation distances in the Mg adlayer systems, which may not perfectly apply to CB

electrons due to the delocalized character of the CB initial-state wave functions[20-22]. Relative time shifts $\Delta\tau[4f - 2p]$ extracted with a robust quantum-mechanical fitting scheme[10-12] (see SI) from streaking spectrograms at different Mg coverages are summarized in Fig. 3a (blue diamonds). They reveal a distinct monotonic increase of $\Delta\tau[4f - 2p]$ with the number of Mg adlayers n - reaching 215 ± 20 as for a 10.4 Å (n = 4) thick Mg film. We verified this trend using a more illustrative analysis that compares the first moments of the streaked W4*f* and Mg2*p* energy distributions as a function of Δt (Fig. 2b, see SI).

The simplest description of the electron propagation is to consider ballistic motion of the centroid of a Bloch wave packet as a free point-like electron in one-dimension[26]. For the Mg layers, $\Delta\tau[4f - 2p]$ is then dominated by the average propagation time τ_{4f} of the 4*f* wave packets traveling at a group velocity $v = \frac{dE(\boldsymbol{k})}{\hbar d\boldsymbol{k}}|_{k=k_0}$. Due to the free-electron-like band-structure of Mg[11,27], we have $\approx \sqrt{2E_{kin}/m_e}$. The kinetic energy of the photoelectrons inside the Mg layer amounts to E_{kin} ~ 93 eV (photon energy $\hbar\omega_{XUV}$ = 118 eV, binding energy of the 4*f* electrons E_b ~32.5 eV, Fermi energy of bulk Mg E_{Fermi} ~7 eV) leading to an average group velocity of $v_{4f} \approx 0.057$ Å/as. We therefore expect τ_{4f} – which is the upper limit for $\Delta\tau[4f - 2p]$ – to increase almost linearly with the number of Mg adlayers n according to $\tau_{4f} \approx n \times d/v_{4f} \approx n \times 45$ as, where d = 2.6 Å is the interlayer spacing of the epitaxial Mg films[13]. A linear fit to the experimental data of Fig. 3a yields a delay of ~42 as per adlayer. The good agreement between experiment and model prediction provides conclusive evidence for the atomic-scale ballistic propagation of the 4*f* electrons being the microscopic origin of the observed time shifts in the spectrograms and corroborates free-electron-like transport in Mg.

This interpretation is substantiated by electron transport simulations[23] of the ballistic motion of the W4*f*, Mg2*p* and CB electrons in the Mg/W(110) systems. Generally, time delays

obtained from such transport calculations are sensitive to i) the average group velocities of the electrons at the relevant energies, ii) their energy-dependent inelastic mean free path $\lambda(E_{kin})$ in the traversed materials and iii) the spatio-temporal profile of the streaking field near the surface[23]. The average group velocities can be deduced from electronic structure calculations [10,18] and all relevant values of $\lambda(E_{kin})$ are known from synchrotron experiments[11] or theory[28]. As a consequence, our experiments open the possibility to explore the spatial variation of the laser field's $E_L(z)$ component normal to the surface (z axis) on an angstrom length scale.

Screening at metallic surfaces becomes effective near the so-called image plane z_{im} located about half layer spacing outside the center of the topmost atomic layer[29,30]. As our method probes the optical near-field at the metal-vacuum interface, the commonly used Fresnel equations based on macroscopic properties of target components with perfectly sharp interfaces cannot be applied. Instead, a phenomenological exponential decay $E_L(z,t) = E_0 e^{-(z-z_{im})/\delta}$ of the surface-normal component of the field inside the material appears to be a reasonable assumption[19,24]. We therefore modelled the impact of different screening lengths δ, i.e. the length scale on which the stepwise prediction of the Fresnel formula does not apply, on the time delays $\Delta\tau[4f - 2p]$ by 1D electron transport simulations (see SI). The time delays $\Delta\tau[4f - 2p]$ predicted by this simple model as a function of n and δ are plotted as green lines in Fig. 3a. Apparently, only the range $0 \leq \delta \leq 3$ Å is compatible with the experiment and the associated error bars, indicating a screening within one atomic layer of Mg.

To scrutinize the origin of this rapid interfacial screening, we employ time-dependent density functional theory (TDDFT)[31] to calculate $E_L(z,t)$ for the Mg/W(110) systems. The surface-

normal component of the incident laser field induces a polarization charge layer at the metal surface which shields the interior of the solid against the external electric field. The centroid of the induced screening charge density (CD) defines the exact position z_{im} of the image plane, which marks the microscopic onset of the local screening process[30] (see Fig. 3b). Both the positions $z_{im}^{(n)}$ and the width $\delta^{(n)}$ of the induced screening charge are found to be almost independent on the number *n* of Mg layers. The key finding is that the laser field is already fully screened at the plane defined by the center of the atoms of the topmost layer for all Mg/W(110) systems, in agreement with the conclusion drawn from the comparison of our experimental data with the phenomenological modelling.

Finally, we incorporate the abrupt screening of the streaking field at the surface revealed by TDDFT in a full 3D streaking simulation[23] of the electron propagation in Mg/W(110) (see SI for a detailed description). Similar to the above-mentioned 1D model, wave packet propagation is simulated by the transport of an ensemble of point-like charges taking stochastic inelastic and elastic scattering events into account. The time delays $\Delta\tau$[4*f* - 2*p*] predicted by these calculations (red squares in Fig. 3a) are in good agreement with the experiment.

Compared to the core-level photoemission time delay $\Delta\tau$[W4*f* - 2*p*] , the temporal shift of the conduction band emission $\Delta\tau$[CB - 2*p*] (Fig. 3c) is distinctly smaller and exhibits a strikingly different dependence on the number of Mg adlayers. A detailed analysis of $\Delta\tau$[CB - 2*p*] within electron transport models is complicated by different (spectrally unresolved) contributions of W(110)- and Mg-derived states to the joint CB feature at $E_{kin} \approx 115$ eV. However, by weighting the excitation probabilities from these different initial states according to their atomic photo-excitation cross sections (see SI), we achieve good overall

agreement with the experimental results, and correctly reproduce the vanishing $\Delta\tau$[CB - 2*p*] time delay for bulk Mg[11]. This suggests that our approximate treatment of the Bloch wave-packet propagation and the dielectric screening response remains valid also for more delocalized initial electronic states – at variance with recent predictions[24,25].

We emphasize that $\Delta\tau$[CB - 2*p*] for n =1 is overestimated in our transport model and lies outside the experimental error margin. A deviation from the semi-classical model appears likely for the Mg/W(110) monolayer system, since strong mixing of band states at the interface may lead to a deviation of the initial-state band structure and excitation cross-sections from their bulk characteristics[25]. A detailed discussion of this phenomenon is beyond the scope of the present study, but indicates the potential of attosecond photoelectron spectroscopy to probe interfacial hybridization between electronic states directly in the time domain and is a first example of applying this technique on phenomena not being accessible to a semi-classical description.

This work extends the realm of attosecond spectroscopy to the direct observation of atomic-scale propagation and damping of electronic and optical wave packets at solid surfaces. The resultant insight into attosecond temporal and – simultaneously – angstrom spatial dimensions opens the door for understanding and exploring electron transport phenomena on the atomic scale and the dielectric response of solids at optical frequencies. Applied to overlayer materials with non-free-electron-like positive-energy states, such a study will shed light on whether stationary band-structure can be used to predict atomic-scale electron propagation on ultra-short time scales. Extrapolation of coverage-dependent streaking spectroscopy to the sub-monolayer regime will provide access to absolute photoemission times and possible intrinsic (atomic) retardation effects in the photoemission process. Beyond

addressing these fundamental questions, attosecond electron transport chronoscopy may prove instrumental in advancing electronic and photonic circuits towards atomic dimensions.

References

1 Bloch, F. Über die Quantenmechanik der Elektronen in Kristallgittern. *Z. Physik* **52**, 555-600, doi:10.1007/BF01339455 (1929).

2 Leo, K., Bolivar, P. H., Brüggemann, F., Schwedler, R. & Köhler, K. Observation of Bloch oscillations in a semiconductor superlattice. *Solid State Communications* **84**, 943-946, doi:http://dx.doi.org/10.1016/0038-1098(92)90798-E (1992).

3 Hentschel, M. *et al.* Attosecond metrology. *Nature* **414**, 509-509 (2001).

4 Drescher, M. *et al.* X-ray Pulses Approaching the Attosecond Frontier. *Science* **291**, 1923-1927 (2001).

5 Schiller, F., Heber, M., Servedio, V. D. P. & Laubschat, C. Electronic structure of Mg : From monolayers to bulk. *Phys. Rev. B* **70**, 125106-125106 (2004).

6 Gremillet, L. *et al.* Time-Resolved Observation of Ultrahigh Intensity Laser-Produced Electron Jets Propagating through Transparent Solid Targets. *Physical Review Letters* **83**, 5015-5018, doi:10.1103/PhysRevLett.83.5015 (1999).

7 Sha, W., Norris, T. B., Schaff, W. J. & Meyer, K. E. Time-resolved ballistic acceleration of electrons in a GaAs quantum-well structure. *Physical Review Letters* **67**, 2553-2556 (1991).

8 Sha, W., Rhee, J.-k., Member, S., Norris, T. B. & Schaff, W. J. Transient Carrier and Field Dynamics in Quantum- Well Parallel Transport : From the Ballistic to the Quasi-Equilibrium Regime. *IEEE Journal of Quantum Electronics* **28** (1992).

9 Shaner, E. & Lyon, S. Picosecond Time-Resolved Two-Dimensional Ballistic Electron Transport. *Physical Review Letters* **93**, 037402-037402, doi:10.1103/PhysRevLett.93.037402 (2004).

10 Cavalieri, A. L. *et al.* Attosecond spectroscopy in condensed matter. *Nature* **449**, 1029-1029 (2007).

11 Neppl, S. *et al.* Attosecond Time-Resolved Photoemission from Core and Valence States of Magnesium. *Physical Review Letters* **109**, 22-26, doi:10.1103/PhysRevLett.109.087401 (2012).

12 Schultze, M. *et al.* Delay in Photoemission. *Science* **328**, 1658-1658 (2010).

13 Aballe, L., Barinov, A., Locatelli, A., Mentes, T. O. & Kiskinova, M. Initial stages of heteroepitaxial Mg growth on W(110): Early condensation, anisotropic strain, and self-organized patterns. *Phys. Rev. B* **75**, 115411-115411 (2007).

14 Mahan, G. D. Theory of Photoemission in Simple Metals. *Physical Review B* **2**, 4334-4350 (1970).

15 Berglund, C. N. & Spicer, W. E. Photoemission Studies of Copper and Silver: Theory. *Physical Review* **136**, A1030-A1044 (1964).

16 Feibelman, P. J. & Eastman, D. E. Photoemission spectroscopy—Correspondence between quantum theory and experimental phenomenology. *Physical Review B* **10**, 4932-4947 (1974).

17 Borisov, a. G., Sánchez-Portal, D., Kazansky, a. K. & Echenique, P. M. Resonant and nonresonant processes in attosecond streaking from metals. *Physical Review B* **87**, 121110-121110, doi:10.1103/PhysRevB.87.121110 (2013).

18 Krasovskii, E. E. Attosecond spectroscopy of solids: Streaking phase shift due to lattice scattering. *Phys. Rev. B* **84**, 195106-195106, doi:10.1103/PhysRevB.84.195106 (2011).

19 Liao, Q. & Thumm, U. Attosecond Time-Resolved Photoelectron Dispersion and Photoemission Time Delays. *Physical Review Letters* **112**, 023602 (2014).

20 Kazansky, A. K. & Echenique, P. M. One-Electron Model for the Electronic Response of Metal Surfaces to Subfemtosecond Photoexcitation. *Phys. Rev. Lett.* **102**, 177401-177401 (2009).

21 Zhang, C. H. & Thumm, U. Attosecond Photoelectron Spectroscopy of Metal Surfaces. *Phys. Rev. Lett.* **102**, 123601-123601 (2009).

22 Zhang, C. H. & Thumm, U. Effect of wave-function localization on the time delay in photoemission from surfaces. *Physical Review A* **84**, 1-4, doi:10.1103/PhysRevA.84.065403 (2011).
23 Lemell, C., Solleder, B., Tökési, K. & Burgdörfer, J. Simulation of attosecond streaking of electrons emitted from a tungsten surface. *Phy. Rev. A* **79**, 62901-62901, doi:10.1103/PhysRevA.79.062901 (2009).
24 Zhang, C. H. & Thumm, U. Probing dielectric-response effects with attosecond time-resolved streaked photoelectron spectroscopy of metal surfaces. *Physical Review A* **84**, 1-7, doi:10.1103/PhysRevA.84.063403 (2011).
25 Vinogradov, N., Marchenko, D., Shikin, A., Adamchuk, V. & Rader, O. Size effects in ultrathin Mg/W(110) films: Quantum electronic states. *Physics of the Solid State* **51**, 179-179 (2009).
26 Kroemer, H. On the group velocity of Bloch waves. *Proceedings of the IEEE* **63**, 988-988, doi:10.1109/PROC.1975.9871 (1975).
27 Bartynski, R. A., Gaylord, R. H., Gustafsson, T. & Plummer, E. W. Angle-resolved photoemission study of the surface and bulk electronic structure of Mg(0001) and Mg(112-bar0). *Phys. Rev. B* **33**, 3644-3644 (1986).
28 Tanuma, S., Powell, C. J. & Penn, D. R. Calculations of electron inelastic mean free paths. IX. Data for 41 elemental solids over the 50 eV to 30 keV range. *Surface and Interface Analysis* **43**, 689-689, doi:10.1002/sia.3522 (2011).
29 Lang, N. D. & Kohn, W. Theory of Metal Surfaces: Induced Surface Charge and Image Potential. *Physical Review B* **7**, 3541-3550 (1973).
30 Liebsch, A. Electronic Screening at Metal Surfaces and the Connection with Physical Phenomena. *Physica Scripta* **35**, 354 (1987).
31 Wachter, G. *et al.* Electron rescattering at metal nanotips induced by ultrashort laser pulses. *Physical Review B* **86**, 035402 (2012).

Supplementary Information is available in the online version of the paper

Acknowledgements

This research was supported by the Munich Center of Advanced Photonics. C.L, G.W. and J.B. acknowledge support by the FWF special research programs SFB-051(ViCoM) and SFB-049 (NextLite) and project P21141-N16. G.W. is supported by the Max Planck Research School of Advanced Photon Science (IMPRS-APS). R.K. acknowledges an ERC Starting Grant. Calculations have been performed on the Vienna Scientific Cluster. S.N. and P.F. thank the Helmholtz Zentrum Berlin for support. We thank P. Echenique, E.E. Krasovskii, A. Kazansky and A.D. Sanchez-Portal for helpful discussions.

Author Contributions

S.N. conceived the material system for this study and performed preparatory experiments. S.N., A.L.C., P.F., E.M., R.E., and R.K. designed and developed the experiment. S.N., R.E. and A.L.C. performed the measurements with the assistance of E.M and E.B. S.N. and R.E. analyzed the data. C.L. and S.N. performed the ballistic electron simulations. G.W. and C.L. performed the TDDFT calculations. M.H. and U.K. developed and prepared the XUV multilayer optics. S.N, R.E, C.L, J.B. and R.K. wrote the manuscript with input from the other authors. R.K. and F.K. initiated the project, R.K., F.K. and P.F. supervised the project. All authors discussed the results and conclusions drawn from them.

Author Information

Correspondence and requests for materials should be addressed to S.N. (sneppl@lbl.gov) and R.K. (reinhard.kienberger@tum.de).

Present address of Stefan Neppl: Lawrence Berkeley National Laboratory, Chemical Sciences Division, 94720 Berkeley, CA, USA.

Figure 1| Spatio-temporal dynamics in attosecond photoemission from Mg/W(110). **a** Principle of the experiment: photoelectrons are launched in a tungsten W(110) crystal and a few-angstrom-thick magnesium (Mg) overlayer by a ~450 as XUV pulse, and are detected in ultra-high vacuum (UHV) with a time-of-flight (TOF) analyzer. At the surface, the arrival times of electrons released from different initial states are probed by streaking their associated electron energy distributions with a $2 \cdot 10^{11}$ W/cm^2 strong electric field delivered by a sub-5 fs broadband p-polarized VIS/NIR laser pulse. Relative time delays $\Delta\tau$ developing during the propagation of the photoelectrons to the metal-vacuum interface are detected as temporal shifts between their laser-dressed energy distributions. The time shifts $\Delta\tau$ are sensitive to the atomic-scale electron transport characteristics (quantified by the inelastic mean free path λ; only indicated for the W4*f* electrons), the Mg overlayer thickness and the screening behavior of the laser field at the solid-vacuum interface. **b** Schematic energy-level diagram for the probed electronic transitions. The central XUV photon energy of ~118 eV allows the simultaneous excitation of Mg2*p*, W4*f* and the joint conduction band (CB) states. A background-corrected photoelectron spectrum of $n = 4$ adlayers Mg on W(110) in the absence of the laser field is shown as black solid line.

Figure 2| Attosecond time-resolved photoemission from Mg/W(110). a Representative streaking spectrogram for $n = 4$ Mg adlayers. All photoelectron spectra are corrected for the inelastic electron background signal. Strength of CB and W4*f* signals are magnified by a factor 6 for better visibility. **b** Exemplary timing analysis of the Mg2*p* and W4*f* core-level electrons: first moments calculated from their respective kinetic energy distributions are shown as crosses (red: Mg2*p*; blue: W4*f*) as a function of NIR-XUV delay Δt. A global fit of the resultant streaking traces to a parameterized waveform for the NIR vector-potential (solid lines) reveals a relative time shift $\Delta\tau[4f - 2p]$, which can be identified with the time delay occurring during the release of the electrons from the metal surface. Insets illustrate the evolution of $\Delta\tau[4f - 2p]$ for $0 < n \leq 4$. Regions exhibiting the largest gradient of the streaking field (corresponding to the highest temporal resolution) are highlighted. An analogous evaluation of $\Delta\tau$[CB - 2*p*] is presented in the supplementary information.

Figure 3| Atomic-scale photoelectron transport and screening of the incident light field. **a** Time delays $\Delta\tau$[4*f* - 2*p*] between the release of W4*f* and Mg2*p* electrons extracted from a large set of streaking spectrograms with different numbers of Mg adlayers are shown as blue diamonds. Error bars denote full standard deviations and are obtained by averaging measurements performed under similar experimental conditions. Fractional adlayers correspond to dispersed 2D islands (on top of a completed Mg layer) that coalesce upon further Mg deposition. Green lines are time delays predicted by our 1D simulation of the photoelectron release dynamics for different screening lengths δ assuming an exponentially decaying normal component of the incident NIR streaking field at the metal-vacuum interface according to $E_L(z,t) = E_0 e^{-(z-z_{im})/\delta}$. The light-green shaded area highlights the screening scenarios compatible with the experiment. Red squares indicate time delays derived from a full 3D electron transport model (red line is a guide to the eyes). **b** Upper panel: illustration of the different screening scenarios for $E_L(z,t)$ considered in **a** on the example of n = 2 Mg adlayers on W(110). The red line is the spatial variation of $E_L(z,t)$ at the interface predicted by TDDFT. Lower panel: snapshot of the NIR-induced charge density (CD) at the metal-vacuum at the maximum of the laser pulse derived by TDDFT (magenta line). The position of the dynamic image plane z_{im} is indicated as black solid line. The lattice potential (averaged parallel to the crystal surface) employed in the DFT calculations is shown as dotted black line. **c** Comparison of time shifts $\Delta\tau$[CB- 2*p*] measured between the emission of CB and Mg2*p* electrons with time delays predicted by the 3D electron transport model.

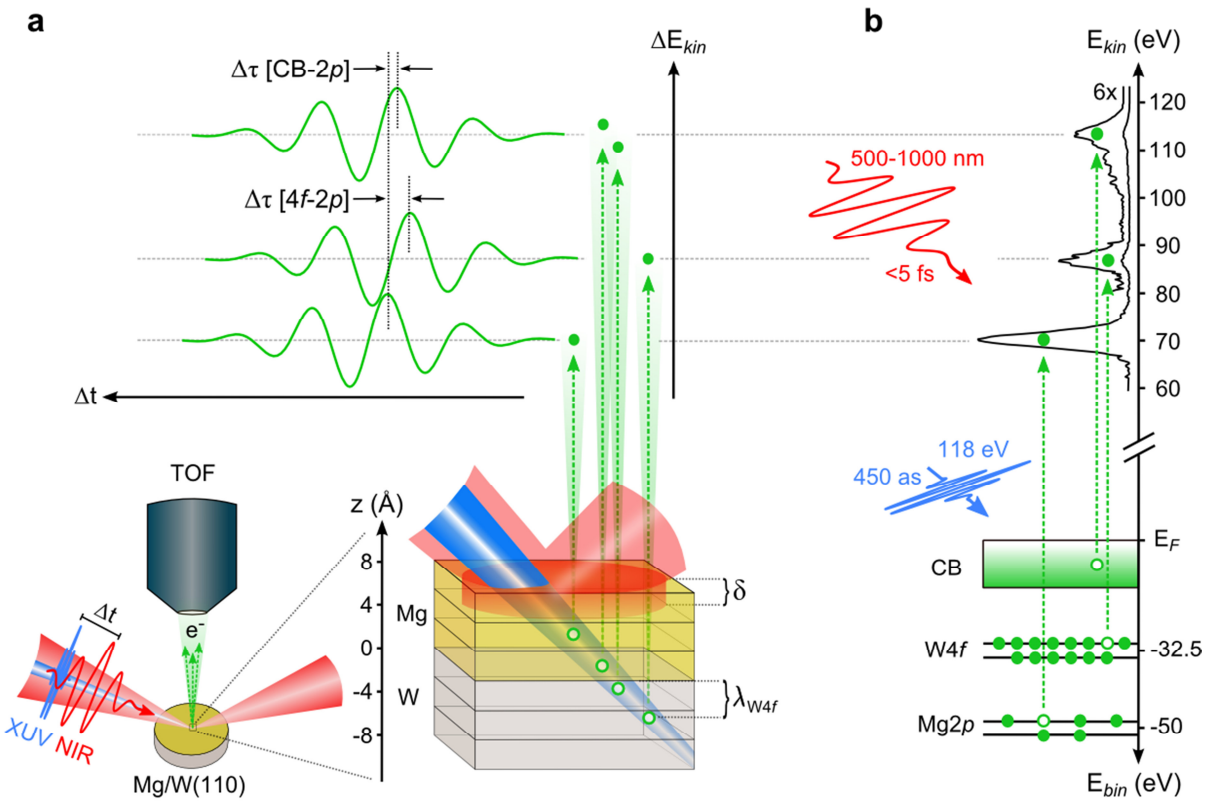
a
b
Δτ [CB-2p]
Δτ [4f-2p]
Δt
ΔE_kin
TOF
e⁻
Δt
XUV
NIR
Mg/W(110)
z (Å)
8
4
0
-4
-8
Mg
W
δ
λ_W4f
E_kin (eV)
6x
120
110
100
90
80
70
60
500-1000 nm
<5 fs
118 eV
450 as
E_F
CB
W4f
-32.5
Mg2p
-50
E_bin (eV)

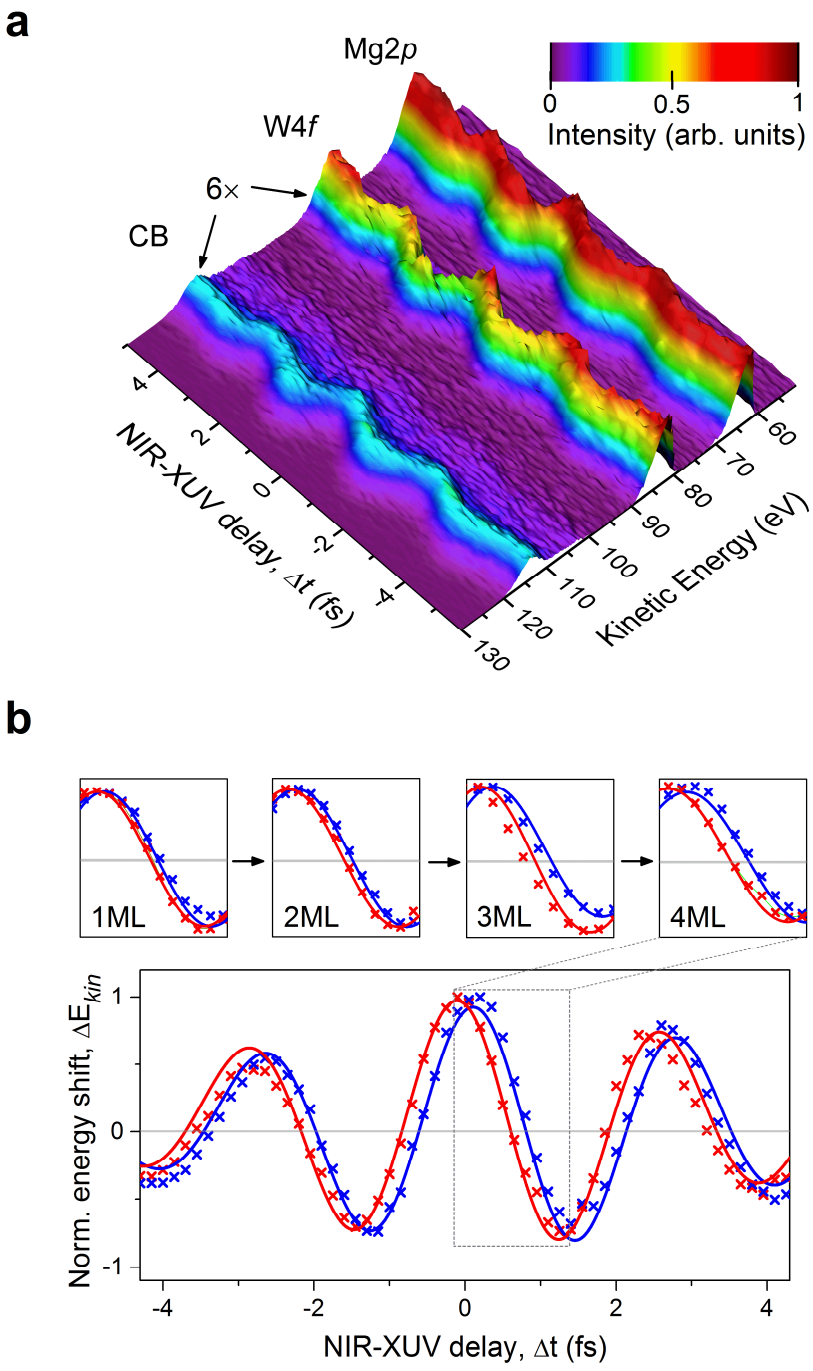
a
Mg2p
W4f
6×
CB
0
0.5
1
Intensity (arb. units)
NIR-XUV delay, Δt (fs)
Kinetic Energy (eV)
b
1ML
2ML
3ML
4ML
Norm. energy shift, ΔE_kin
NIR-XUV delay, Δt (fs)

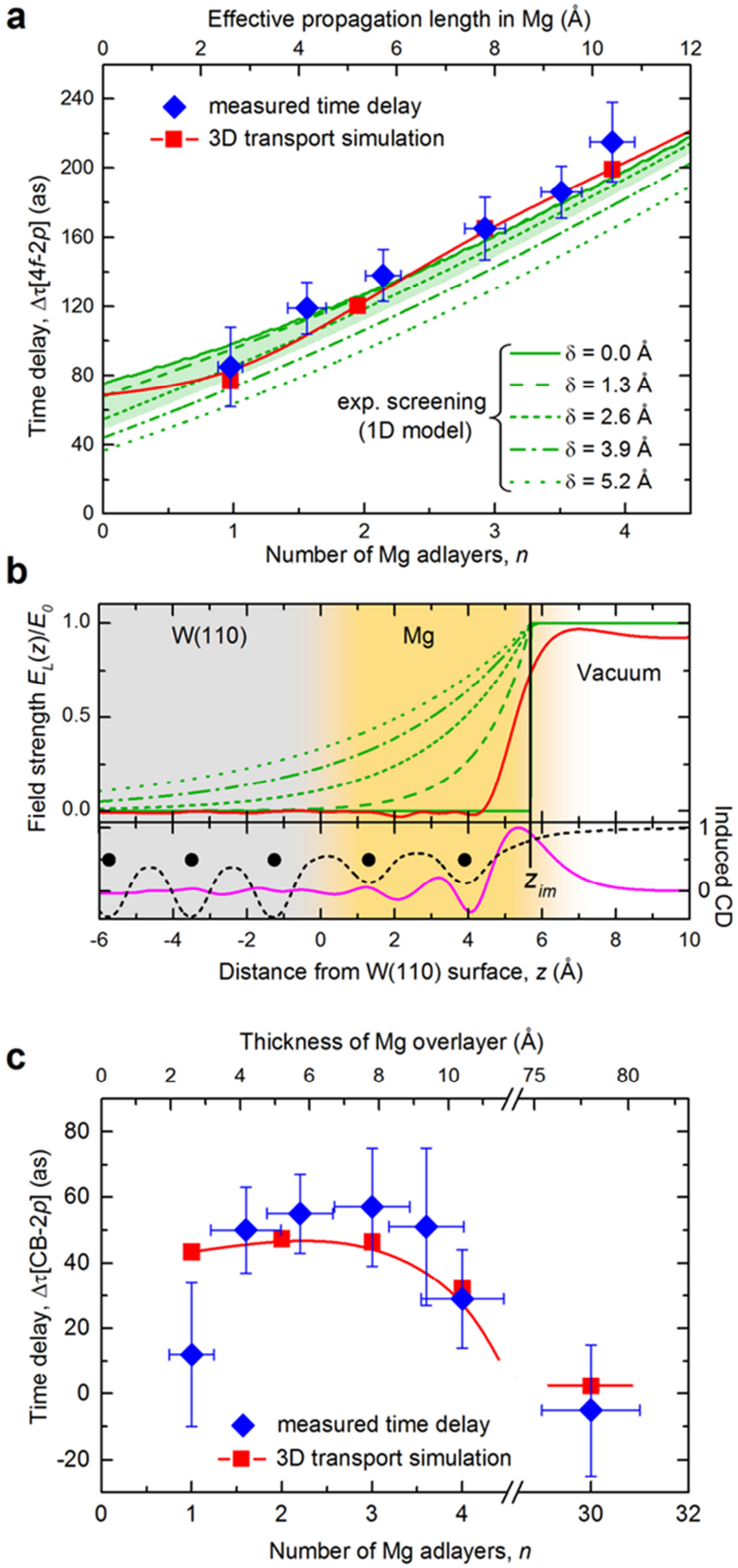
a
Effective propagation length in Mg (Å)
measured time delay
3D transport simulation
Time delay, Δτ[4f-2p] (as)
exp. screening
(1D model)
δ = 0.0 Å
δ = 1.3 Å
δ = 2.6 Å
δ = 3.9 Å
δ = 5.2 Å
Number of Mg adlayers, n
b
W(110)
Mg
Vacuum
Field strength E_L(z)/E_0
Induced CD
z_im
Distance from W(110) surface, z (Å)
c
Thickness of Mg overlayer (Å)
Time delay, Δτ[CB-2p] (as)
measured time delay
3D transport simulation
Number of Mg adlayers, n